Biomass Conversion and Biorefinery
https://doi.org/10.1007/s13399-022-02720-w

ORIGINAL ARTICLE

Utilization of biochar prepared by invasive plant species *Alternanthera philoxeroides* to remove phenanthrene co-contaminated with PCE from aqueous solutions

Xin Liu[1] · Qing Wang[1] · Xin Song[1,2] · Kang Li[3] · Mukhtiar Ali[1,2] · Changlong Wei[1] · Jilu Che[1] · Siwei Guo[1] · Xuedan Dou[1]

Received: 17 January 2022 / Revised: 8 April 2022 / Accepted: 20 April 2022
© The Author(s), under exclusive licence to Springer-Verlag GmbH Germany, part of Springer Nature 2022

Abstract

In this study, a novel and environmental-friendly biochar prepared by alien species, *Alternanthera philoxeroides* (*AP*) under a temperature range of 300–700˚C (BC300-BC700), was applied to remove phenanthrene (PHE), perchloroethylene (PCE), and PHE/PCE bi-contaminant from aqueous solutions. Interestingly, the maximum adsorption capacity of *AP* biochar changed nonlinearly as the pyrolysis temperature increased, with BC400 and BC300 having the highest maximum adsorption capacities of 2.83 and 2.13 mg/g, respectively, followed by BC700, BC500, and BC600. The sorption kinetics of PHE and PCE on BC300 under single- and bi-contaminant conditions can be described by pseudo-second-order and pseudo-first-order kinetic models, respectively. In addition, it was observed that PHE and PCE could be removed simultaneously by BC300, and the presence of PHE inhibited the maximum sorption capacity of PCE onto *AP* biochar. Furthermore, this study revealed that the functional groups of C-O, C = O, and C = C played a key role in the removal of PHE/PCE from bi-contaminant solutions. These findings suggested that pyrolysis of invasive plants can be an option to control invasive plants and also contribute to the adsorption of organic contaminants for contaminant remediation.

Keywords Biochar · Bi-contaminant · Phenanthrene · Perchloroethylene · *Alternanthera philoxeroides*

1 Introduction

Biochar is a carbon-rich solid formed by the pyrolysis of biomass and other substances under oxygen-free or oxygen-limited conditions, which might provide a solution for waste recycling and carbon neutralization in the environment [1, 2]. Biochar has a strong adsorption capacity due to its large surface area, rich pore structure, and the sorption characteristics of its surface functional groups [3–5]. Various studies have shown that biochar is an ecofriendly sorption material for the removal of heavy metals, organic pollutants, and inorganic contaminants in soil and aqueous environments [2]. The utilization of plant biomass as biochar has been considered as an approach, such as wood and agricultural wastes that are commonly used as raw materials for the preparation of biochar, and all have shown some level of efficacy in pollutant removal [4]. In addition, invasive plants have also been used to prepare biochar [6, 7], which caters to both the environmental benefits and economic values.

China has experienced tremendous invasive alien species to the establishment and spread resulting from the international communications. *Alternanthera philoxeroides* (*AP*),

Highlights
1. Biochar pyrolyzed by intrusive species *AP* can remove compound organic contaminants.
2. *AP* biochar prepared at 300 ~400℃ has better adsorption performance.
3. Competitive sorption was observed in PHE/PCE bi-contaminant solutions.
4. The maximum sorption capacity of PCE onto *AP* biochar was inhibited by PHE.
5. C=C, C-O, and C=O of biochar accounted for the chemisorption of binary contaminants.

✉ Qing Wang
qwang@issas.ac.cn

[1] CAS Key Laboratory of Soil Environment and Pollution Remediation, Institute of Soil Science, Chinese Academy of Sciences, Nanjing 210008, China

[2] University of Chinese Academy of Sciences, Beijing 100049, China

[3] No.1 Institute of Geo-Environment Survey of Henan, Henan 450003, China

Published online: 11 May 2022

originated from Brazil, has been recognized in the first batch of invasive alien species in China and can habituate in the southeastern part of China at the end of this century in prediction [8]. *AP* usually grows rapidly in wetland ecosystems, which will not only block waterways but also further threaten biodiversity [9, 10]. The traditional control strategy for *AP* is artificial harvesting, but this practice is limited by the high costs of removing and disposing of large amounts of biomass [10, 11]. Moreover, disposal of the harvested material by natural decomposition might release pathogens and methane, which further influence climate change globally [12]. Therefore, seeking appropriate solutions for the treatment and utilization of invasive plants has attracted interests in environmental agricultural studies [10]. Alien species *AP* have been used as a cost-effective raw material for biochar preparation [10]. Pharmaceutical and personal care products like ibuprofen and Pb (II) have been successfully adsorbed by biochar prepared from *AP* [9, 10]. Moreover, *AP* biochar has the potential to be integrated with other materials like incorporating with bentonite to efficiently remove Cd (II) or modified by hydrogen peroxide to adsorb metformin hydrochloride [13, 14].

Polycyclic aromatic hydrocarbons (PAHs) have been identified as persistent organic pollutants (POPs) and are the most widely detected organic contaminants in groundwater due to their common use in industrial processes [15, 16]. The maximum reported concentration of naphthalene in groundwater is 97.10 mg/L at a chemical site, which was 97.10 times the standard limit for class III water quality according to Groundwater Quality Standard GB/T 14848–2017 (100 μg/L) [17–19]. Another group of POPs, chlorinated aliphatic hydrocarbons (CAHs), are also frequently detected in groundwater and have been applied as industrial solvents, degreasing agents, and dry-cleaning agents for several decades, although they may be carcinogenic to humans [20–22]. A former dry-cleaning facility in Denmark has detected a perchloroethylene (PCE) concentration of up to 62 mg/L in groundwater [20]. Groundwater resources, especially in former industrial sites, are often contaminated by several types of contaminants [23]. In a municipal landfill site in China, CAH and PAH concentrations of up to 2.80 and 2.19 μg/L, respectively, were detected in groundwater [24]. Due to the ecological and environmental risks generated by PAHs and CAHs in aqueous environments, it is crucial for their removal [25]. Therefore, using *AP* as biochar source materials for PAHs and CAHs could be an appropriate solution for pollution treatment and the efficient utilization of invasive plants. None of the studies have explored the sorption of PAHs and CAHs on *AP* biochar.

The structural properties of biochar determine the removal mechanism of contaminants in the environment. By increasing the aromatic and hydrophobic properties of biochar, a strong adsorption capacity for hydrophobic organic contaminants such as PAHs and CAHs has been attained [4, 26]. Bonds such as C=O and C-O are the functional groups in the sorption of contaminants [27]. Other pathways, such as van der Waals forces, London dipole, π stacking, partition, pore-filling, and intra-particle (internal) diffusion, also contribute to the sorption of organic contaminants. For example, the adsorption of PCE onto biochar occurs through partitioning and pore-filling processes [28]. Most studies have focused on the adsorption of a single contaminant, with only a few studies considering the simultaneous sorption of bi-contaminant by biochar. Competition or stimulation phenomena between different contaminants might occur in media contaminated by multiple pollutants [4]. Most of the effects of bi-contaminant on each other in the sorption process remain unclear.

This study aimed to investigate the ability of *AP* biochar to remove phenanthrene (PHE) and PCE, two representatives of PAHs and CAHs, respectively, from aqueous solutions. Batch sorption experiments were conducted to study the adsorption abilities of single PHE by *AP* biochar prepared at different pyrolytic temperatures ranging from 300 to 700˚C (BC300-BC700). *AP* biochar's sorption mechanisms of single PHE and binary PHE mixed with PCE were investigated through the characterization of biochar before and after the experiment by X-ray photoelectron spectroscopy (XPS), X-ray diffraction analysis (XRD), and Fourier transform infrared spectrometer (FTIR).

2 Materials and methods

2.1 Preparation of *Alternanthera philoxeroides* biochar

The stem and leaves of invasive alien species *AP* were used to prepare biochar in reference to previous methods [12, 13]. *Alternanthera philoxeroides* was washed with tap water followed by deionized water and then dried at 50˚C in an oven. The dried *AP* was then ground, sieved, and transferred to a tube furnace for pyrolysis preparation under a flow of nitrogen. The *AP* samples were heated from room temperature to 100˚C and kept for 30 min. To prepare *AP* biochar with different pyrolytic temperatures, the *AP* biochar was heated from 100˚C increasing at a constant rate of 4˚C/min to the target temperatures of 300, 400, 500, 600, and 700˚C, and kept for 2 h at each target temperature, and the obtained biochar was designated as BC300, BC400, BC500, BC600, and BC700, respectively.

2.2 Batch sorption experiment

2.2.1 Single contaminant adsorption experiment

Batch experiments were carried out to study the adsorption processes of PHE and PCE on *AP* biochar. The first experiment was carried out to study the adsorption of PHE by

AP biochar prepared with different pyrolysis temperatures (300–700˚C: BC300-BC700), and the second experiment examined the adsorption of PHE/PCE bi-contaminant onto BC300. For all experiments, the analytical data attained a mean value using three replicates (n = 3), which were analyzed alongside blank controls without *AP* biochar. The adsorption kinetics of PHE on BC300-BC700 were determined at 25˚C in a shaker (MQL-621R, Minquan, China) at 150 rpm. Phenanthrene (analytical grade, Aladdin, China) was accurately weighed and dissolved into acetonitrile (gradient grade, Supelco, USA) at 10 g/L as the stock solution, and then diluted with deionized water to a final concentration of 1 mg/L in 50 mL vials. To study the adsorption kinetics of PHE on BC300-BC700, the concentration of PHE was 1 mg/L with the addition of 10 mg AP biochar into a 10-mL aqueous solution and the reaction intervals ranged from 10 min to 24 h. The method was followed by previous studies [29]. Approximately 1 mL of the supernatant was collected, extracted by acetonitrile, and filtered for further analysis by high-performance liquid chromatography (HPLC, Shimadzu LC-20AT, Japan) using an instrument equipped with a fluorescence detector (FLD). Adsorption isotherms were obtained at a rate of 150 rpm at 25˚C for 12 h after adsorption equilibrium. The initial concentrations of PHE were in the range of 0.05, 0.1, 0.2, 0.4, 0.6, 0.8, and 1 mg/L with 10 mg *AP* biochar in a 10-mL aqueous solution. After equilibration, the PHE concentration remaining in the solution was determined by HPLC.

2.2.2 Bi-contaminant adsorption experiment

For the bi-contaminant experiment, the stock solution of PCE (analytical grade, Yonghuachem, China) was diluted to 1 mg/L and mixed with PHE solution in 50 serum bottles capped with Teflon-lined rubber septa and aluminum crimp caps. Similar to the setup of the first experiment, the reaction intervals of the adsorption kinetics ranged from 10 min to 24 h with 1 mg/L PHE and 20 mg of BC300 was added to each serum bottle of 20 mL. For the adsorption isotherms of PHE with PCE, the initial PHE concentrations were in the range of 0.05, 0.1, 0.2, 0.4, 0.6, 0.8, and 1 mg/L. The PCE concentration was determined by gas chromatography (GC, Agilent 7820A, USA) equipped with a headspace sampler (7697A, Agilent, USA).

The pH of aqueous solutions was determined by Mettler Toledo (FE20, China). As indicated by previous studies, unlike active carbon, *AP* biochar is not a pH-dependent adsorbent and the adsorption capacity shall be smoothly saturated around pH 7 [12, 30]. For all experiments in this study, the pH values of the solutions before and after the biochar adsorption were about 7 and 10, respectively. The initial condition suits the progress of reactions because of the weak competition of H^+ binding with the functional groups (hydroxyl, carboxyl, carbonyl, etc.) and the strong precipitation of anions (OH^-, CO_3^{2-}, etc.) [13].

2.3 Characterization of *Alternanthera philoxeroides* biochar

Scanning electron microscopy (SEM, SU8010, Hitachi, Japan) was applied to observe the surface and pore structures of *AP* biochar. Brunauer–Emmett–Teller (BET) analyzer (ASAP2460, Micromeritics Instrument Corp, America) was applied to analyze the specific surface area and pore structure of biochar. XRD (Ultima IV, Rigaku, Japan) was applied to determine the crystal condition, crystal phase, crystal structure, and bonding state of *AP* biochar. The surface bonds on the *AP* biochar were analyzed by FTIR (Nicolet 6700, Thermo Fisher Scientific, USA) with an IR scanned area of 400–4000 cm^{-1}. XPS (K-Alpha, Thermo Fisher Scientific) was applied to test the elemental content and morphology on the surface of *AP* biochar.

2.4 Analysis of PHE and PCE

The mobile phase of the HPLC analysis was a 50% methanol aqueous solution, at a flow rate of 1.4 mL/min. The column was an Agilent PN A7000250X046 (250 × 4.6 mm). With a ratio of 1:1, the water phase (A) and the organic phase (B) were ultrapure water and acetonitrile, respectively [29, 31]. The PCE concentration was determined by GC in the aqueous samples with an electron capture detector (ECD) followed our previous studies [32]. The injection volume was 1 µL, and the injection was performed in split mode (split ratio 20:1). The column adopted was Agilent DB–624 (60 m × 0.25 mm × 1.4 µm), with a temperature range of 60–260˚C. High-purity N_2 was used as a carrier gas with a velocity of 1 mL/min. The temperature of the ECD was 320˚C. The oven temperature increased from 40˚C (maintained for 5 min) to 100˚C at 8˚C/min and was then continually increased to 200˚C at 15˚C/min, where it was held for 2 min.

2.5 Data analysis

The formula used to calculate the adsorption amount Q_e (Eq. (1)) of PHE and PCE onto *AP* biochar was as follows [33]:

$$Q_e = \frac{(C_0 - C_e)V}{m} \quad (1)$$

where C_0 and C_e are the initial and final (equilibrium) concentrations (mg/L) of contaminants in the solution, respectively; V is the volume of the solution (mL); and m is the mass of *AP* biochar (mg).

Pseudo-first-order, pseudo-second-order, and internal diffusion kinetic models were selected to fit the analytical results of the *AP* biochar adsorption of PHE and PCE. The pseudo-first-order model was as follows [33, 34]:

$$Q = Q_e\left(1 - e^{-K_1 t}\right) \tag{2}$$

$$v_1 = K_1 Q_e \tag{3}$$

The pseudo-second-order model was as follows [35]:

$$\frac{t}{Q} = \frac{1}{K_2} Q_e^2 + \frac{t}{Q_e} \tag{4}$$

$$v_2 = K_2 Q_e^2 \tag{5}$$

The internal diffusion model was as follows [36]:

$$Q = K_i t^{0.5} + C_i \tag{6}$$

where t is the contact time (h), Q and Q_e are the adsorption capacities (mg/g) of PHE and PCE on the *AP* biochar at intervals and at equilibrium, respectively; $K_1\left(h^{-1}\right)$ and K_2 $(g/mg \cdot h))$ are the rate constants of the pseudo-first-order and the pseudo-second-order models, respectively; $v_1 (mg/(g \cdot h))$ and $v_2\, mg^2/\left(g^2 \cdot h\right)$ are the adsorption rates; $K_i\,(mg/g \cdot h^{0.5})$ is the internal diffusion constant of stage i; and C_i is the constant of stage i, which characterizes the boundary layer effect during the diffusion process. The larger the value of C_i, the greater the boundary layer effect will be.

Freundlich and Langmuir models were used to fit the isotherm adsorption data [37]. The Langmuir model is as follows:

$$Q_e = \frac{Q_m b \rho_e}{1 + b\rho_e} \tag{7}$$

The Freundlich model is as follows:

$$Q_e = K_L \rho_e^n \tag{8}$$

where ρ_e is the concentration of contaminants in solution at equilibrium (mg/L); Q_m is the maximum adsorption capacity of *AP* biochar (mg/g); and b is the adsorption constant of the Langmuir model, which usually applies to the monolayer adsorption model. The Freundlich model is an empirical model, which applies to low- and medium-concentration chemicals. K_L is the adsorption capacity, and n is an empirical index in the Freundlich model.

3 Results and discussion

3.1 Adsorption of single-contaminant PHE on BC300–BC700

3.1.1 Adsorption kinetics of PHE on BC300–BC700

As shown in Fig. 1(a), the PHE adsorption kinetics of BC300–BC700 shared similar trends, with only slight differences. Overall, the adsorption amount of PHE increased over time, indicating the effectiveness of PHE removal by *AP* biochar. The adsorption rates of PHE on BC300–BC700 were initially fast in the first 1 h and then slowed and gradually approached an equilibrium. Similar trends were observed in previous studies [5, 9, 38]. The initial rapid adsorption might be attributable to a large number of sorption sites available on the external surface of *AP* biochar [21]. Chemisorption, involving changes in bond energies leading to changes in functional groups, occurred simultaneously [39]. As the surface sorption sites were gradually saturated during the sorption process, PHE slowly diffused into the porous material and the accompanying chemisorption slowed down [9]. As a result, the adsorption rate of PHE onto *AP* biochar slowed and eventually tended toward an adsorption equilibrium.

As shown in Fig. 1(b) and (c), the adsorption kinetics data for PHE on BC300–BC700 were fitted with a pseudo-first-order kinetics model and pseudo-second-order kinetics model. The adsorption kinetics model parameters used are given in Table 1. The pseudo-second-order kinetic model achieved better fitting than the pseudo-first-order model according to the coefficient of determination (R^2), indicating that the adsorption process fitted the pseudo-second-order model well. This suggested that the adsorption process of PHE on BC300–BC700 might involve a chemisorption interaction between PAHs ions and polar functional groups on the adsorbent, such as ion exchange and a chelating reaction [40–42]. In addition, BC700 had the highest equilibrium adsorption capacity of 0.810 mg/g, followed by BC300 with 0.640 mg/g in the pseudo-second-order kinetic model. The other three *AP* biochar had relatively lower adsorption capacities in comparison.

Figure 1(d) shows the fitting result of the Weber and Morris internal diffusion model. The linear fitting of the internal diffusion model was adjusted to the experimental data divided into two stages. The first stage with a large slope was the diffusion process, and the second stage with a small slope was associated with the surface adsorption in the sorption process [43]. This indicated that the first stage was strongly involved in the control of the sorption process, while the second stage did not pass through the origin, indicating that internal diffusion was not the only process controlling sorption [43, 44]. The adsorption kinetics indicated that the sorption of PHE onto BC300–BC700 was determined by surface adsorption and internal diffusion together, which was consistent with the results of other studies [40, 45, 46].

3.1.2 Adsorption isotherm of PHE on BC300–BC700

The Langmuir and Freundlich models were used to fit the data for PHE adsorption on BC300–BC700, as shown in Fig. S1(a) and (b). The resulting regression

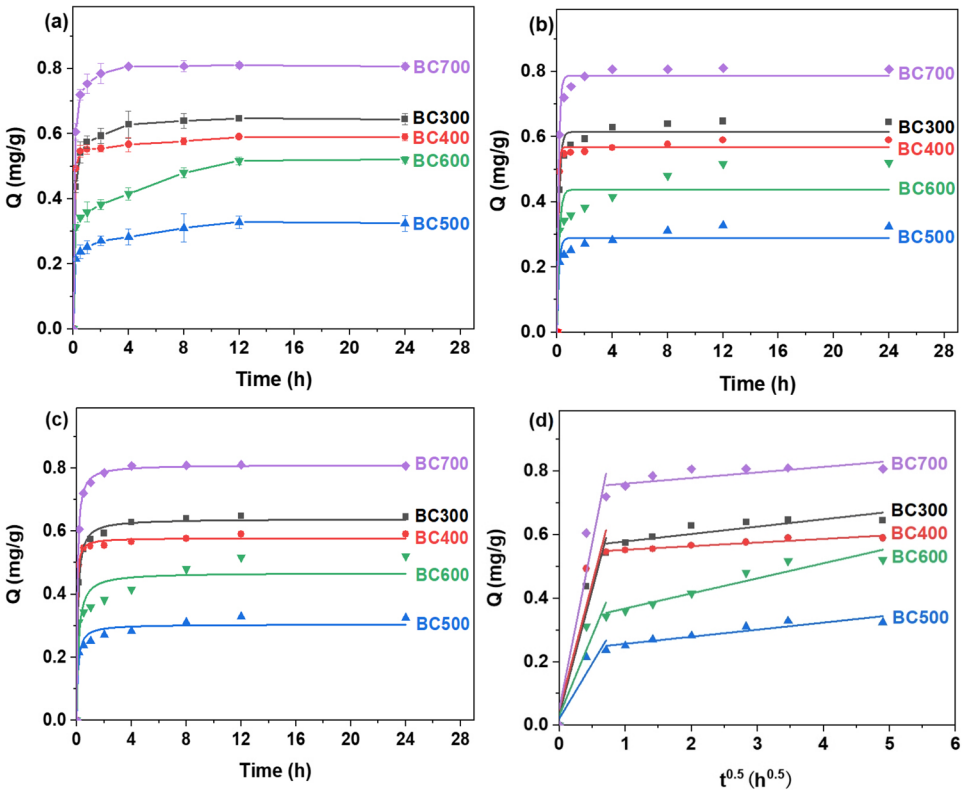

Fig. 1 **a** Adsorption kinetics of PHE onto BC300–BC700 and fittings of **b** the pseudo-first-order kinetic model, **c** the pseudo-second-order kinetic model, and **d** the internal diffusion model

parameters are listed in Table 2. The Langmuir model indicated that monolayered sorption took place on a homogeneous sorbent surface, while the Freundlich model indicated that adsorption occurred on heterogeneous surfaces and the binding sites were not equal [40, 47, 48]. The gradient of the initial concentration was set below 1 mg/L, which was commonly selected in previous studies because the solubility of PHE is low in groundwater [48, 49]. In general, there was an improvement in adsorption capacity with an increase in the initial PHE concentration. In brief, as suggested by the R^2 values, the adsorption isotherms of PHE by *AP* biochar prepared at low temperatures (300–500˚C) were a better fit using the Langmuir model, indicating the dominance of single molecular layer adsorption in the sorption of PHE onto *AP* biochar. In contrast, BC600 and BC700 had higher R^2 values in the Freundlich model, indicating the presence of multiple molecular layer adsorption in the sorption of PHE onto *AP* biochar prepared at high temperatures (600–700˚C).

Table 1 Adsorption kinetics parameters of PHE sorption onto BC300–BC700

Models	Parameters	Unit	BC300	BC400	BC500	BC600	BC700
Pseudo-first-order kinetic	Q_e	mg/g	0.610	0.570	0.290	0.440	0.790
	K_1	1/h	6.90	12.1	7.25	6.16	8.47
	v_1	mg/(g·h)	4.21	6.90	2.10	2.71	6.69
	R^2		0.974	0.993	0.899	0.823	0.987
Pseudo-second-order kinetic	Q_e	mg/g	0.640	0.580	0.300	0.470	0.810
	K_2	g/(mg·h)	18.9	57.9	33.8	15.8	21.1
	v_2	$mg^2/(g^2 \cdot h)$	7.74	19.5	3.04	3.49	13.8
	R^2		0.996	0.997	0.952	0.901	0.999
Internal diffusion model	K_1	kg/ $(mg \cdot h^{0.5})$	0.0350	0.0500	0.0220	0.0320	0.0530
	C_1		0.790	0.800	0.350	0.500	1.05
	R^2		0.878	0.770	0.767	0.763	0.841
	K_2	kg/ $(mg \cdot h^{0.5})$	0.560	0.540	0.230	0.320	0.740
	C_2		0.0230	0.0110	0.0220	0.0470	0.0180
	R^2		0.676	0.896	0.837	0.895	0.483

Table 2 Isotherm parameters of PHE sorption onto BC300–BC700

Biochar	Langmuir			Freundlich		
	b (L/mg)	Q_{max} (mg/g)	R^2	K_L	1/n	R^2
BC300	5.78	2.13	0.980	3.75	0.700	0.960
BC400	2.72	2.83	0.958	3.49	0.830	0.935
BC500	4.34	0.460	0.935	0.410	0.390	0.787
BC600	10.7	0.410	0.957	0.440	0.390	0.983
BC700	14.1	1.94	0.968	3.95	0.590	0.989

In the Langmuir model, BC400 and BC300 had the highest maximum adsorption capacities of 2.83 and 2.13 mg/g, respectively, followed by BC700 with 1.94 mg/g. In contrast, BC500 and BC600 had very limited maximum adsorption capacities of 0.460 and 0.410 mg/g, respectively. This suggested a potential change in the pore structure and surface functional group compositions such as -OH when the pyrolysis temperature reached a certain point. In addition, the relatively low K_L and 1/n value (< 0.5) of BC500 and BC600 indicated that the adsorption of PHE was not ideal. It has been reported that biochar is composed of both carbonized organic matter (COM) and amorphous organic matter (AOM) [50, 51]. Usually, a higher pyrolysis temperature improves the carbonization of biochar and decreases the proportion of AOM [51], therefore improving the sorption performance of biochar on target contaminants [52, 53]. However, this study identified a different phenomenon in which the adsorption capacity of contaminants by *AP* biochar might not increase linearly along with the *AP* biochar's pyrolysis temperature. This phenomenon was also found in a previous study by Kim, Lee and Khim [54], in which a peat moss-derived biochar did not show an increase in its adsorption capacity when its pyrolysis temperature increased.

3.1.3 Sorption mechanisms of PHE on BC300–BC700

It has been reported the adsorption ability of biochar was affected by surface features and functional groups [55, 56]. Therefore, the study used SEM, XRD, BET, and FTIR to investigate the physical and chemical properties of the biochar. Indicated by the SEM images (5 µm to 50 µm) of BC300 in Fig. S2, the ability of *AP* biochar to adsorb PHE and PCE was benefited from its surface features of irregular shapes and rough surface area. Furthermore, the well-developed pores in biochar have been enriched with the mineral crystallinity and aromatic arrangements, which was consistent with the previous studies that identified the dense fibers on the unique macrocellular morphology and surface precipitation ability of biochar [57, 58].

In general, the presence of functional groups such as C = O, -OH, and C = C, which were influenced by the pyrolysis temperature, has an influence on the adsorption capacity of PHE in aqueous solutions. The XRD spectra of BC300–BC700 *AP* biochar prior to the sorption of PHE were scanned from 10° to 80° at a scan rate of 0.02° per second. The spectra from 22° to 43° are shown in Fig. 2(a), with no relatively broad amorphous diffraction peaks observed in this range. In contrast, many sharp crystal diffraction peaks were observed in this range. A comparison conducted with Jade software showed that the characteristic peaks of 2θ at 28.34° and 40.50° were the crystal peaks of a potassium salt (KCl) (JCPDS NO. 75–0296), which is a common component in *AP* biochar prepared by plants and crops [59, 60]. Additionally, with a change in the pyrolysis temperature during the *AP* biochar preparation process, there were slight differences in the chemical bonds within the *AP* biochar. The C–O peaks at 29.30° and 31.30° shifted slightly in the spectra. In addition, the peaks at 24.30° and 30.94° in the XRD patterns represented quartz (silica) and graphite, including C = O and -OH functional groups, as suggested in a previous study [61]. These peaks indicated the formation of aromatic carbon in the *AP* biochar, which enabled the adsorption of PHE [62, 63].

An FTIR analysis in the 4000–400 cm^{-1} spectral region was used to identify the bonds of BC300–BC700, with the results presented in Fig. 2(b). The FTIR peak characteristics of *AP* biochar obtained at different pyrolysis temperatures were similar, and only a few peaks were observed to be absent. There were strong sorption peaks at 3420 cm^{-1} in all *AP* biochar, which were the stretching vibrations of the -OH bond [64]. The sorption peak at 2850 cm^{-1} situated in the 2845–2865 cm^{-1} spectral region was related to the C-H bond stretching vibration of aliphatic hydrocarbons or cycloalkanes, as a part of the asymmetric and symmetric CH_2-C-H structure [61]. The peak at 1620 cm^{-1} was suggested to be the stretching vibration of the C = C bond and was related to the characteristic peaks of the benzene ring or aromatics [40, 64, 65]. The peaks at 1380 and 1118 cm^{-1} were associated with -CH_2 and C-O vibrations, respectively [40].

As indicated by Table 2, BC300 and BC400 have the largest adsorption capacities, with the strongest peaks at 3420 cm^{-1} and 1620 cm^{-1} accordingly. Meanwhile, the relatively lower intensity peaks at 3420 cm^{-1} (-OH) and at 1620 cm^{-1} (C = C) were observed in BC500 and BC600, which indicated their weak representative

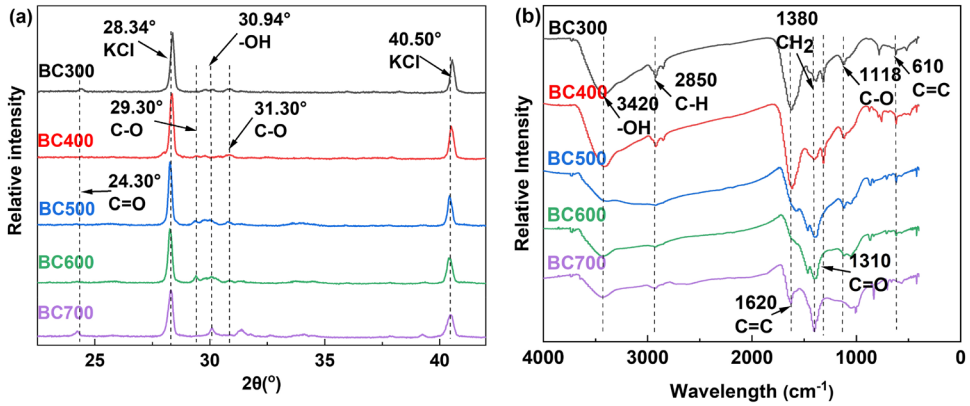

Fig. 2 **a** XRD diffraction spectrum and **b** FTIR spectrum of BC300–BC700

aromatic and nonpolar structures, in which π–π interactions with planar and aromatic PAHs were more common when compared with other biochar [66]. Previous studies have shown that free radicals (·OH) in the AP biochar may be able to form reactive oxygen species (e.g., -OH) and remove organic contaminants [67, 68]. Therefore, FTIR results showed a decrease in -OH and -COOH concentration and better carbonization of *AP* biochar when the pyrolysis temperature exceeded 500˚C [69, 70]. These changed characteristics might explain why BC500 and BC600 had a lower maximum adsorption capacity than the other *AP* biochar. When the pyrolysis temperature was raised to 700 °C, the C = C aromatic structures in BC700 at 1620 cm^{-1} reinforced, which might be due to the gradual thermal cracking of cellulose in the biomass as the temperature increased and the gradual condensation of aliphatic hydrocarbons into aromatic rings during the dehydration process [28]. The peak intensities of C = O at 1310 cm^{-1} and C-O at 1118 cm^{-1} showed obvious decreasing trends when the pyrolysis temperature was increased from 300 to 700˚C, indicating the increase in carbonization and aromatic structures when the pyrolysis temperature reached a certain temperature, while the decreasing number of free-radicals indicated the removal of contaminants.

3.2 Sorption of PHE/PCE bi-contaminant on BC300

3.2.1 Sorption of PHE (bi-contaminant) on BC300

The adsorption isotherm results revealed that the maximum adsorption capacities of BC300 and BC400 were superior to those of the other *AP* biochar. The adsorption capacity of BC300 was higher than that of BC400 at the initial concentration of 1 mg/L PHE. In addition, BC300 was prepared at the lowest pyrolysis temperature and therefore had the lowest energy demand. Therefore, BC300 was chosen for further studies to investigate the sorption of PHE/PCE bi-contaminant onto *AP* biochar.

Figure 3(a) shows the adsorption kinetics for BC300 to adsorb PHE in single- and bi-contaminant solutions. In general, similar behaviors were observed in the sorption of both solutions. The adsorption rate of PHE in the bi-contaminant was slower, with 66.5% of the ultimate adsorption occurring in the first 60 min, whereas the corresponding figure for a single solute was 89.1%. The adsorption capacity then continued to increase at a slow speed to reach an equilibrium at 12 h. The presence of PCE reduced the adsorption capacity of PHE onto *AP* biochar in the first 12 h. Then, in the next 12 h when equilibrium was reached, the adsorption capacity of PHE in bi-contaminant solutions was slightly larger than in its single solution, reaching levels of 0.664 and 0.648 mg/g, respectively. Therefore, it could be speculated that the adsorption of PCE and PHE onto *AP* biochar occur simultaneously and the presence of PCE did not have an obvious impact on the sorption of PHE on BC300.

Figure 3(b) and (c) shows the pseudo-first-order and pseudo-second-order kinetic models of adsorption onto *AP* biochar. The detailed kinetics parameters are presented in Table 3. The adsorption process of PHE onto BC300 was better fitted in the pseudo-second-order model, with the initial adsorption rates for PHE in both single- and bi-contaminant conditions reaching 7.86 and 5.87 $mg^2/(g^2 \cdot h)$, respectively, which indicated that the addition of PCE reduced the adsorption rate of PHE and had a negative impact on the absorptivity of BC300. The equilibrium adsorption capacity of single PHE onto BC300 was 0.640 mg/g, which was slightly higher than that of the PHE in the bi-contaminant solution (0.600 mg/g).

The internal diffusion model is presented in Fig. 3(d). The regression of Q_e and $t^{1/2}$ was linear, but it did not pass through the origin, indicating that the involvement of the internal diffusion process was not the main rate-limiting step for the sorption of PHE onto *AP* biochar in the first stage. It was apparent that other processes, such as the initial external mass transfer or chemical reactions, were also involved [71]. In comparison with a single contaminant solution (0.550 $kg/(mg \cdot h^{0.5})$), the bi-contaminant condition had a lower K_i value

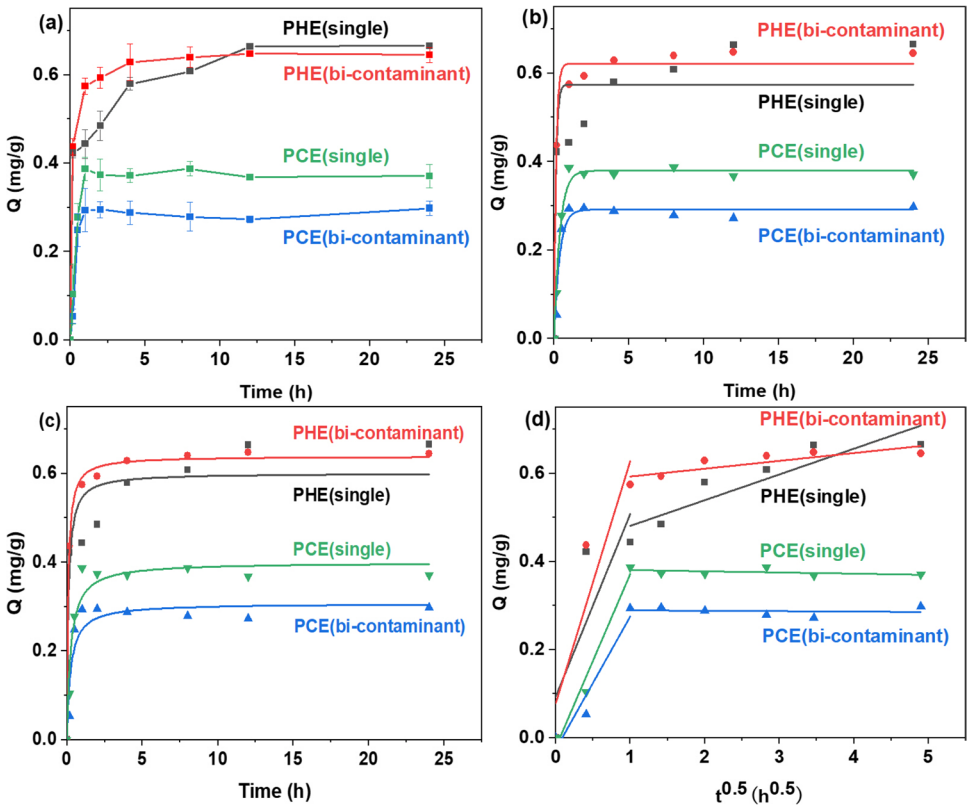

Fig. 3 **a** Adsorption kinetics of PHE and PCE onto BC300 in bi-contaminant aqueous solutions and fittings of **b** the pseudo-first-order kinetic model; **c** the pseudo-second-order kinetic model; **d** the internal diffusion model

Table 3 Adsorption kinetics parameters of PHE and PCE on BC300

Models	Parameters	Unit	PHE (single)	PHE (bi-contaminant)	PCE (single)	PCE (bi-contaminant)
Pseudo-first-order kinetic	Q_e	mg/g	0.622	0.575	0.380	0.292
	K_1	1/h	7.26	7.91	2.57	2.71
	v_1	mg/(g·h)	4.52	4.55	0.977	0.791
	R^2		0.987	0.871	0.985	0.954
Pseudo-second-order kinetic	Q_e	mg/g	0.640	0.600	0.307	0.400
	K_2	g/(mg·h)	19.2	16.3	13.3	10.1
	v_2	$mg^2/(g^2 \cdot h)$	7.86	5.87	1.25	1.62
	R_2		0.996	0.895	0.884	0.935
Internal diffusion model	K_1	$kg/(mg \cdot h^{0.5})$	0.550	0.414	0.393	0.302
	C_1		0.0790	0.0940	-0.0212	-0.0259
	R_2		0.850	0.694	0.976	0.941
	K_2	$kg/(mg \cdot h^{0.5})$	0.0178	0.0584	-0.0269	-0.00928
	C_2		0.575	0.423	0.383	0.290
	R_2		0.711	0.831	0.208	0.0179

($0.414\ kg/(mg \cdot h^{0.5})$) in the first stage. It can be speculated that the addition of PCE deaccelerated the adsorption rate of PHE on the surface of BC300 particles, as reflected by the K_i value [60]. This phenomenon might be due to the small PCE molecules being mobile and able to diffuse into *AP* biochar faster than PHE molecules during the particle diffusion stage [54]. The second stage of the internal diffusion model showed that the sorption of PHE on BC300 increased with the presence of PCE, as the K_i value of PHE in bi-solute at the second stage was higher than that in the single solute solutions.

The Langmuir and Freundlich isothermal models were used to describe the adsorption isotherms, as shown in Fig. S3. In general, the adsorption capacity increased as the concentrations of PHE and PCE increased, which was due to the ratio of the number of adsorbate moiety to the available active sites on the external surface of adsorbent increasing accordingly [72, 73]. Table 4 lists the adsorption isotherm parameters for PHE sorption onto BC300. Higher R^2 values were observed for the Langmuir isotherm models, suggesting that the adsorption isotherm of PHE with PCE could be better described by the Langmuir model. The maximum adsorption capacities of PHE alone and PHE with PCE onto BC300 were 2.13 and 2.03 mg/g, respectively. This indicated that the presence of PCE would not significantly affect the maximum adsorption capacity of PHE onto *AP* biochar. Furthermore, for the Freundlich model, because the K_L value under bi-contaminant conditions was larger than under single contaminant conditions, the sorption affinity or bond energy of the sorption between adsorbates and adsorbents was speculated to be reduced due to the addition of PCE [60].

3.2.2 Sorption of PCE in a bi-contaminant solution on BC300

In addition to the impact of PCE on PHE in the sorption process, the impacts of PHE on PCE were also studied. Figure 3(a) shows the adsorption kinetics of PCE on BC300 for single and bi-contaminant solutions. Similar to previous studies, the PCE adsorption on *AP* biochar was found to be initially rapid (first hour) with or without PHE, which could be attributed to the strong sorption on the external surface of the *AP* biochar [21]. As the sorption progressed, PCE diffused into the pores to reach the internal surface of BC300 and then gradually reached an equilibrium.

The adsorption kinetics fitting curves of PCE onto BC300 are shown in Fig. 3(b), (c), and (d). The kinetic fitting parameters are listed in Table 3. In general, the pseudo-first-order kinetic model fitted the data better than the pseudo-second-order model, indicating that the sorption of PCE from both single and bi-contaminant solutions was predominantly a physical partitioning process [59, 74]. Compared with the adsorption rate of PHE at 4.52 and 4.55 mg/(g·h) in single- and bi-contaminant conditions, respectively, the adsorption rate of PCE was slower at 0.977 and 0.791 mg/(g·h), respectively. As a volatile organic contaminant, PCE relied on the pore diffusion process to achieve its partition into *AP* biochar, which naturally had a slower adsorption rate than that of PHE [21]. The equilibrium adsorption capacity of PCE decreased from 0.380 mg/g for a single contaminant solution to 0.292 mg/g for a bi-contaminant solution. Therefore, there was a competition between PCE and PHE for the sorption sites on BC300, and the addition of PHE into PCE solution suppressed the adsorption capacity and adsorption rate of PCE onto *AP* biochar.

As shown in Fig. 3(d) and Table 3, the regression of Q_e and $t^{1/2}$ was also linear, and it passed close to the origin. Therefore, the internal diffusion process was significant in the sorption of PCE from both single- and bi-contaminant solutions in the first stage. The low K_i values in the second stage indicated that it was more difficult for PCE to diffuse into BC300 internally after equilibrium was reached. Notably, the R^2 values for PCE under single- and bi-contaminant conditions were relatively low in the second stage. The reason for this was that after the equilibrium of PCE on BC300 was reached (1 to 24 h), the equilibrium concentrations C_e were almost parallel to the X-axis, which generated extremely low R^2 values. However, the low R^2 values did not necessarily mean that the regression model lacked credibility.

3.2.3 Sorption mechanism of PHE and PCE on BC300

Both XRD and FTIR analyses were undertaken to study the characteristics of *AP* biochar pre- and post-sorption. As shown by the results of an XRD analysis in Fig. 4(a), in addition to the disappeared or weakened crystal peaks of KCl at 28.34° and 40.50°, which may have been due to KCl being in a crystalline state and has been supersaturated in the solution and was washed off, the C-O bond also disappeared at 31.30° [75]. In addition, the BET analysis result in Table S2 shows that BC300 contained K (11.5%) and Cl (5.2%), which was also confirmed in the XRD analysis. Figure 4(b) shows the FTIR spectra for the sorption of single PHE, single PCE, and the PHE/PCE bi-contaminant on BC300. After adsorbing the three groups of contaminants, the peak intensities of the -OH and C = O functional groups changed slightly, which was related to the chemical groups present. Compared with BC300 before the sorption, the peak intensities of -OH at 3420 cm^{-1} increased after the sorption of the single PHE, single PCE, and PHE/PCE bi-contaminant, while the C-O peak at 1118 cm^{-1} disappeared. This indicated that the C-O

Table 4 Isothermal adsorption parameters of PHE in the presence of PCE on BC300

Contaminant	Langmuir			Freundlich		
	b (L/mg)	Q_m (mg/g)	R^2	K_L	1/n	R^2
PHE (single)	5.78	2.13	0.980	3.75	0.703	0.960
PHE (bi-contaminant)	4.42	2.03	0.999	3.48	0.762	0.998

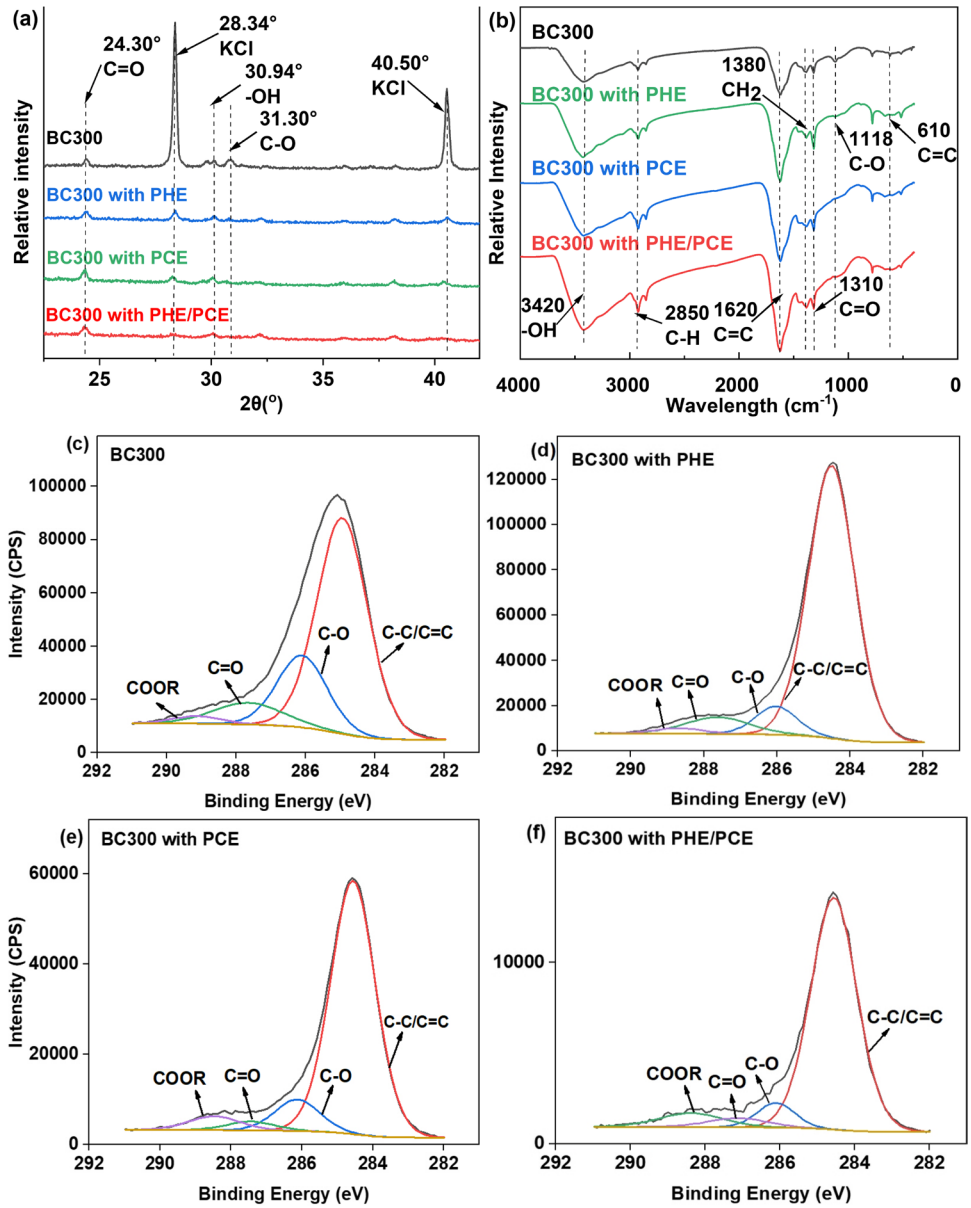

Fig. 4 **a** XRD diffraction spectrum and **b** FTIR spectrum of BC300 before and after sorption; XPS C1s peaks of **c** BC300, BC300 post-sorption with **d** PHE, **e** PCE, and **f** bi-contaminant PHE/PCE

bond participated in chemical reactions, and the breakage of the C-O bond might be the main contributor to the sorption of PHE and PCE. Therefore, both FTIR and XRD produced the same experimental results, with a cross-verification of the importance of C-O in the sorption of PHE and PCE by *AP* biochar. This phenomenon indicated the possible occurrence of specific cation–π and hydrogen–π interactions in the presence of K^+ and functional groups (i.e., –COOH) in the *AP* biochar [76, 77].

It has been reported that hydrophobic interactions, including partitioning, van der Waals forces, and the π–π, hydrogen–π, and cation–π interactions between PHE and *AP* biochar, commonly dominate the sorption of PHE onto *AP* biochar [28, 39, 78]. In this study, the molar O/C and (O + N)/C ratios (Table S2), indicators of the polarity of carbonaceous materials such as -OH and -COOH groups [79, 80], suggested that BC300 was less aromatic and more hydrophilic, compared with biochar prepared in previous studies [81, 82], which was likely due to the less extent of carbonization and abundance of polar functional groups. Furthermore, studies have pointed out that low-temperature (e.g., 300˚C) pyrolyzed *AP* biochar would have obvious PAHs partitioning and van der Waals force properties because of the *AP* biochar's polarity [28, 83].

On the other hand, given that *AP* biochar contained a C = C bond as implied by the π = π interactions, PCE might interact with the aromatic content in the *AP* biochar [84]. However, PCE has no active hydrogen atom and was therefore unable to interact internally, specifically with polar functional groups [28, 85]. Therefore, the adsorption

capacity of PCE onto BC300, which was polar and hydrophilic, was limited due to the missing hydrogen functional groups (i.e., –COOH and -OH), which explained the smaller adsorption capacity of PCE than PHE onto BC300 under single-solute conditions. Importantly, the lack of internal interactions between hydrogen atoms in PCE and polar functional groups of BC300 might explain the difficulty in internal diffusion during the second stage of the internal diffusion models, which further supported the phenomenon that the loading of PCE into PHE solution did not decrease the adsorption capacity of PHE onto BC300 as discussed above.

The functional groups' composition of BC300 before and after the sorption process was investigated by XPS to quantitatively measure the changes in bonds [86]. As shown in Fig. S4, all the spectra presented similar characteristic peaks that were mainly assigned to C1s, but the peak intensities under bi-contaminant PHE/PCE conditions in XPS analysis were particularly low, indicating that C and O atoms were more actively to mediating contaminants in the sorption. The peak of C–C/C = C, C-O, and C = O bonds decreased significantly in the bi-contaminant solution, indicating their intensive reactions with PHE and PCE simultaneously. The XPS results suggested that no shift of bonds was observed and the most predominant peak occurred at 284.9 eV for the C–C/C = C bond [87–89]. As suggested above, PCE was intended to interact with the aromatic part of *AP* biochar. The decrease in peak intensities of the C–C/C = C bond in Fig. 4(c) and (e) supported the speculation that PCE was adsorbed by *AP* biochar. In contrast, C–C/C = C may be less influenced in the sorption of PHE by *AP* biochar, as indicated in Fig. 4(c) and (d). The other main C1s peaks for BC300 were C-O, C = O, and COOR, with binding energies of 286.1, 287.5, and 289.1 eV, respectively [60, 87]. The decreased intensities of C–C/C = C, C-O, and C = O functional groups in Fig. 4(f) revealed their participation in the sorption of PHE/PCE bi-contaminant solution.

The parameters of XPS results are detailed in Table S1. The relative ratio of C = O peaks decreased from 21.87% before the sorption to less than 10% after the sorption of single PHE, single PCE, and bi-contaminant PHE/PCE. Meanwhile, the relative proportions of C-O and COOR were low and only slightly changed before and after the sorption process, while the proportion of C–C/C = C increased from 66.7% to over 80% after the sorption process. This phenomenon implies that C–C/C = C bond is still the main component in BC300, though experienced significant decrease of peak area of characteristic peak. A previous study observed similar ratio changes, which suggested a breakage of C = O functional groups on the surface of BC300 after sorption, and thus, its chemical characteristics became more aromatic and less hydrophilic [90]. Additionally, the dominant C bonds of BC300 were C = C, C-O, and C = O, which were consistent with the elemental compositions of C (61.2%) and O (16.6%) in BC300 as presented in Table S2. Therefore, according to the analysis results of FTIR and XPS, C = C, C-O, and C = O functional groups have played a key role in the chemisorption of PHE/PCE bi-contaminant solution.

4 Conclusions

The performance of biochar pyrolyzed by intrusive species *AP* to remove single- and bi-contaminant PHE and PCE from aqueous solutions was investigated. The adsorption of PHE on BC300–BC700 fitted the pseudo-second-order model well. The adsorption isotherms were a better fit with the Langmuir model for BC300–BC500 and the Freundlich model for BC600–BC700. The maximum adsorption capacity of PHE followed the order of BC400 > BC300 > BC700 > BC500 > BC600. Under the bi-contaminant PHE/PCE conditions, the pseudo-second-order model and pseudo-first-order kinetic model better described the adsorption kinetics of PHE and PCE on BC300, respectively. Notably, the presence of PCE did not significantly inhibit the maximum adsorption capacity of PHE onto *AP* biochar. According to the analysis results of FTIR and XPS, it was found that C = C, C-O, and C = O played a dominant role in PHE/PCE bi-contaminant's sorption on BC300.

Through the pyrolysis process at a relative low temperature 300˚C, the organic matters and biomass of *AP* have been transformed into BC300, which was found to be a promising adsorbent for the removal of co-contaminants of PAHs and CAHs. The successful application of *AP* biochar provides an eco-friendly and low-cost approach for the re-utilization of harmful weeds. Moreover, the use of *AP* biochar is an effective alternative to traditional control measures to reduce the growth of *AP* without further environmental damage. In a nutshell, the economic benefits from the re-utilization of *AP* as biochar to adsorb organic contaminants are promising.

Supplementary Information The online version contains supplementary material available at https://doi.org/10.1007/s13399-022-02720-w.

Acknowledgements We acknowledge for all materials and financial supports. This research was supported by the Youth Foundation of the National Natural Science Foundation of China, China (No. 41701365), the Major Program of the National Natural Science Foundation of China, China (No. 41991335), the Jiangsu Provincial Key Research and Development Program, China (No. BE2019624), and the Ecological and Environmental Research Program of Jiangsu Province, China (No. 2020001).

Author's Contribution Xin Liu did data curation, methodology, and writing original draft. Qing Wang performed conceptualization, editing, review, supervision, and funding acquisition. Xin Song edited and reviewed the article. Kang Li done investigation and resources. Mukhtiar Ali investigated and reviewed the article. Changlong Wei was involved in funding acquisition, editing, and review. Jilu Che done investigation and resources. Siwei Guo investigated the study. Xuedan Dou did resources.

Declarations

Ethics approval Not applicable.

Conflict of interest The authors declare no relevant financial or non-financial interests to disclose that could have appeared to influence the work reported in this paper.

References

1. Khan N, Chowdhary P, Gnansounou E, Chaturvedi P (2021) Biochar and environmental sustainability: Emerging trends and techno-economic perspectives. Bioresour Technol 332:125102
2. Singh A, Sharma R, Pant D, Malaviya P (2021) Engineered algal biochar for contaminant remediation and electrochemical applications. Sci Total Environ 774:145676
3. Zhang X, Miao X, Xiang W, Zhang J, Cao C, Wang H, Hu X, Gao B (2021) Ball milling biochar with ammonia hydroxide or hydrogen peroxide enhances its adsorption of phenyl volatile organic compounds (VOCs). J Hazard Mater 403:123540
4. Papageorgiou A, Azzi ES, Enell A, Sundberg C (2021) Biochar produced from wood waste for soil remediation in Sweden: Carbon sequestration and other environmental impacts. Sci Total Environ 776:145953
5. Yuan P, Wang J, Pan Y, Shen B, Wu C (2019) Review of biochar for the management of contaminated soil: Preparation, application and prospect. Sci Total Environ 659:473–490
6. Li SB, Dong LJ, Wei ZF, Sheng GD, Du K, Hu BW (2020) Adsorption and mechanistic study of the invasive plant-derived biochar functionalized with CaAl-LDH for Eu(III) in water. J Environ Sci 96:127–137
7. Nguyen XC, Nguyen TTH, Nguyen THC, Le QV, Vo TYB, Tran TCP, La DD, Kumar G, Nguyen VK, Chang SW, Chung WJ, Nguyen DD (2021) Sustainable carbonaceous biochar adsorbents derived from agro-wastes and invasive plants for cation dye adsorption from water. Chemosphere 282:131009
8. Tu W, Xiong Q, Qiu X, Zhang Y (2021) Dynamics of invasive alien plant species in China under climate change scenarios. Ecol Indic 129:107919
9. Wang X, Jing Y, Cao Y, Xu S, Chen L (2019) Effect of chemical aging of Alternanthera philoxeroides-derived biochar on the adsorption of Pb(II). Water Sci Technol 80:329–338
10. Du Y.-d, Zhang X.-q, Shu L, Feng Y, Lv C, Liu H.-q, Xu F, Wang Q, Zhao C.-c, Kong Q (2020) Safety evaluation and ibuprofen removal via an Alternanthera philoxeroides-based biochar. Environ Sci Pollut Res 28:40568–40586
11. You W, Yu D, Xie D, Han C, Liu C (2014) The invasive plant Alternanthera philoxeroides benefits from clonal integration in response to defoliation. Flora 209:666–673
12. Yang Y, Wei Z, Zhang X, Chen X, Yue D, Yin Q, Xiao L, Yang L (2014) Biochar from Alternanthera philoxeroides could remove Pb(II) efficiently. Bioresour Technol 171:227–232
13. Jing YD, Cao YQ, Yang QQ, Wang X (2020) Removal of Cd(II) from Aqueous Solution by Clay-biochar Composite Prepared from Alternanthera philoxeroides and Bentonite. BioResources 15:598–615
14. Huang X, Liu Y, Liu S, Li Z, Tan X, Ding Y, Zeng G, Xu Y, Zeng W, Zheng B (2016) Removal of metformin hydrochloride by Alternanthera philoxeroides biomass derived porous carbon materials treated with hydrogen peroxide. RSC Adv 6:79275–79284
15. Pierro L, Matturro B, Rossetti S, Sagliaschi M, Sucato S, Alesi E, Bartsch E, Arjmand F, Papini MP (2017) Polyhydroxyalkanoate as a slow-release carbon source for in situ bioremediation of contaminated aquifers: From laboratory investigation to pilot-scale testing in the field. New Biotechnol 37:60–68
16. Huang B, Lei C, Wei C, Zeng G (2014) Chlorinated volatile organic compounds (Cl-VOCs) in environment — sources, potential human health impacts, and current remediation technologies. Environ Int 71:118–138
17. Qiao X, Zheng B, Li X, Zhao X, Dionysiou DD, Liu Y (2021) Influencing factors and health risk assessment of polycyclic aromatic hydrocarbons in groundwater in China. J Hazard Mater 402:123419
18. Miao Y, Kong X-S, Li C-Z (2019) Distribution and Sources of Polycyclic Aromatic Hydrocarbons in a Karst Groundwater System in a Strongly Industrial City. Huanjing Kexue 40:239–247
19. Jin A, He J, Chen S, Huang G (2014) Distribution and transport of PAHs in soil profiles of different water irrigation areas in Beijing. China Environ Sci Processes Impacts 16(1526):1534
20. Guleria A, Chakma S (2021) Fate and contaminant transport model-driven probabilistic human health risk assessment of DNAPL-contaminated site. Environ Sci Pollut Res 28:14358–14371
21. Xiang W, Zhang X, Chen K, Fang J, He F, Hu X, Tsang DCW, Ok YS, Gao B (2020) Enhanced adsorption performance and governing mechanisms of ball-milled biochar for the removal of volatile organic compounds (VOCs). Chem Eng J 385:123842
22. Lai A, Aulenta F, Mingazzini M, Palumbo MT, Papini MP, Verdini R, Majone M (2017) Bioelectrochemical approach for reductive and oxidative dechlorination of chlorinated aliphatic hydrocarbons (CAHs). Chemosphere 169:351–360
23. Hu G, Liu H, Chen C, Li J, Hou H, Hewage K, Sadiq R (2021) An integrated geospatial correlation analysis and human health risk assessment approach for investigating abandoned industrial sites. J Environ Manage 293:112891
24. Han DM, Tong XX, Jin MG, Hepburn E, Tong CS, Song XF (2013) Evaluation of organic contamination in urban groundwater surrounding a municipal landfill, Zhoukou, China. Environ Monit Assess 185:3413–3444
25. Wickrama-Arachchige AUK, Guruge KS, Inagaki Y, Tani H, Dharmaratne TS, Niizuma Y, Ohura T (2021) Halogenated polycyclic aromatic hydrocarbons in edible aquatic species of two Asian countries: Congener profiles, biomagnification, and human risk assessment. Food Chem 360:9
26. Hassan M, Liu Y, Naidu R, Parikh SJ, Du J, Qi F, Willett IR (2020) Influences of feedstock sources and pyrolysis temperature on the properties of biochar and functionality as adsorbents: A meta-analysis. Sci Total Environ 744:140714
27. Fan Q, Sun J, Chu L, Cui L, Quan G, Yan J, Hussain Q, Iqbal M (2018) Effects of chemical oxidation on surface oxygen-containing functional groups and adsorption behavior of biochar. Chemosphere 207:33–40
28. Schreiter IJ, Schmidt W, Schüth C (2018) Sorption mechanisms of chlorinated hydrocarbons on biochar produced from different feedstocks: Conclusions from single- and bi-solute experiments. Chemosphere 203:34–43
29. Shen R-Y, Luo Y-M, Feng S, Zhang G-Y, Wu L-H, Li Z-G, Teng Y, Christie P (2009) Benzo a pyrene and Phenanthrene in Municipal Sludge from the Yangtze River Delta, China. Pedosphere 19:523–531
30. Wang X-S, Qin Y (2006) Removal of Ni(II), Zn(II) and Cr(VI) from aqueous solution by Alternanthera philoxeroides biomass. J Hazard Mater 138:582–588
31. Kottuparambil S, Agusti S (2020) Cell-by-cell estimation of PAH sorption and subsequent toxicity in marine phytoplankton. Chemosphere 259:127487
32. Tang S, Song X, Wang Q, Wang S (2020) Effects of two surfactants on microbial diversity of a PCE-degrading microbial consortium. Chemosphere 261:127685

33. Hyder AHMG, Begum SA, Egiebor NO (2015) Adsorption isotherm and kinetic studies of hexavalent chromium removal from aqueous solution onto bone char. J Environ Chem Eng 3:1329–1336
34. Salvestrini S (2019) A modification of the Langmuir rate equation for diffusion-controlled adsorption kinetics. React Kinet Mech Catal 128:571–586
35. Ho YS, McKay G (1999) Pseudo-second order model for sorption processes. Process Biochem 34:451–465
36. Heaney N, Ukpong E, Lin C (2020) Low-molecular-weight organic acids enable biochar to immobilize nitrate. Chemosphere 240:124872
37. Tang D, Zheng Z, Lin K, Luan J, Zhang J (2007) Adsorption of p-nitrophenol from aqueous solutions onto activated carbon fiber. J Hazard Mater 143:49–56
38. Sun T, Xu Y, Sun Y, Wang L, Liang X, Jia H (2021) Crayfish shell biochar for the mitigation of Pb contaminated water and soil: Characteristics, mechanisms, and applications. Environ Pollut 271:116308
39. Fu H, Wei C, Qu X, Li H, Zhu D (2018) Strong binding of apolar hydrophobic organic contaminants by dissolved black carbon released from biochar: A mechanism of pseudomicelle partition and environmental implications. Environ Pollut 232:402–410
40. Tang J, Lv H, Gong Y, Huang Y (2015) Preparation and characterization of a novel graphene/biochar composite for aqueous phenanthrene and mercury removal. Bioresour Technol 196:355–363
41. Zhou Z, Liu YG, Liu SB, Liu HY, Zeng GM, Tan XF, Yang CP, Ding Y, Yan ZL, Cai XX (2017) Sorption performance and mechanisms of arsenic(V) removal by magnetic gelatin-modified biochar. Chem Eng J 314:223–231
42. Ahmed W, Mehmood S, Núñez-Delgado A, Ali S, Qaswar M, Shakoor A, Mahmood M, Chen D-Y (2021) Enhanced adsorption of aqueous Pb(II) by modified biochar produced through pyrolysis of watermelon seeds. Sci Total Environ 784:147136
43. Ronix A, Pezoti O, Souza LS, Souza IPAF, Bedin KC, Souza PSC, Silva TL, Melo SAR, Cazetta AL, Almeida VC (2017) Hydrothermal carbonization of coffee husk: Optimization of experimental parameters and adsorption of methylene blue dye. J Environ Chem Eng 5:4841–4849
44. Lopes GKP, Zanella HG, Spessato L, Ronix A, Viero P, Fonseca JM, Yokoyama JTC, Cazetta AL, Almeida VC (2021) Steam-activated carbon from malt bagasse: Optimization of preparation conditions and adsorption studies of sunset yellow food dye. Arab J Chem 14:103001
45. Lawal AA, Hassan MA, Zakaria MR, Yusoff MZM, Norrrahim MNF, Mokhtar MN, Shirai Y (2021) Effect of oil palm biomass cellulosic content on nanopore structure and adsorption capacity of biochar. Bioresour Technol 332:125070
46. Wang K, Sun Y, Tang J, He J, Sun H (2020) Aqueous Cr(VI) removal by a novel ball milled Fe0-biochar composite: Role of biochar electron transfer capacity under high pyrolysis temperature. Chemosphere 241:125044
47. Hammo MM, Akar T, Sayin F, Celik S, Akar ST (2021) Efficacy of green waste-derived biochar for lead removal from aqueous systems: Characterization, equilibrium, kinetic and application. J Environ Manage 289:112490
48. Cao H, Zhang P, Jia W, Wang C, Xing B (2021) Adsorption of phenanthrene onto magnetic multi-walled carbon nanotubes (MMWCNTs) influenced by various fractions of humic acid from a single soil. Chemosphere 277:130259
49. Li W, Zhu X, He Y, Xing B, Xu J, Brookes PC (2013) Enhancement of water solubility and mobility of phenanthrene by natural soil nanoparticles. Environ Pollut 176:228–233
50. Cornelissen G, Gustafsson Ö, Bucheli TD, Jonker MTO, Koelmans AA, van Noort PCM (2005) Extensive Sorption of Organic Compounds to Black Carbon, Coal, and Kerogen in Sediments and Soils: Mechanisms and Consequences for Distribution, Bioaccumulation, and Biodegradation. Environ Sci Technol 39:6881–6895
51. Chen B, Zhou D, Zhu L (2008) Transitional Adsorption and Partition of Nonpolar and Polar Aromatic Contaminants by Biochars of Pine Needles with Different Pyrolytic Temperatures. Environ Sci Technol 42:5137–5143
52. Bianco F, Race M, Papirio S, Oleszczuk P, Esposito G (2021) The addition of biochar as a sustainable strategy for the remediation of PAH–contaminated sediments. Chemosphere 263:128274
53. Beesley L, Moreno-Jiménez E, Gomez-Eyles JL, Harris E, Robinson B, Sizmur T (2011) A review of biochars' potential role in the remediation, revegetation and restoration of contaminated soils. Environ Pollut 159:3269–3282
54. Kim J, Lee SS, Khim J (2019) Peat moss-derived biochars as effective sorbents for VOCs' removal in groundwater. Environ Geochem Health 41:1637–1646
55. Godlewska P, Schmidt HP, Ok YS, Oleszczuk P (2017) Biochar for composting improvement and contaminants reduction. A review. Bioresour Technol 246:193–202
56. Pan XQ, Gu ZP, Chen WM, Li QB (2021) Preparation of biochar and biochar composites and their application in a Fenton-like process for wastewater decontamination: A review. Sci Total Environ 754:142104
57. Reza MS, Afroze S, Bakar MSA, Saidur R, Aslfattahi N, Taweekun J, Azad AK (2020) Biochar characterization of invasive Pennisetum purpureum grass: effect of pyrolysis temperature. Biochar 2:239–251
58. Bashir S, Zhu J, Fu Q, Hu H (2018) Comparing the adsorption mechanism of Cd by rice straw pristine and KOH-modified biochar. Environ Sci Pollut Res 25:11875–11883
59. Liu L, Fan S (2018) Removal of cadmium in aqueous solution using wheat straw biochar: effect of minerals and mechanism. Environ Sci Pollut Res 25:8688–8700
60. Zhang Y, Zhang J, Chen F, Ma H, Chen D (2020) Influence of biochar with loaded metal salts on the cracking of pyrolysis volatiles from corn straw. Energy Sources Part A: Recovery, Utilization, and Environmental Effects 1–10
61. Rahman MA, Lamb D, Rahman MM, Bahar MM, Sanderson P, Abbasi S, Bari ASMF, Naidu R (2021) Removal of arsenate from contaminated waters by novel zirconium and zirconium-iron modified biochar. J Hazard Mater 409:124488
62. Chutia RS, Kataki R, Bhaskar T (2014) Characterization of liquid and solid product from pyrolysis of Pongamia glabra deoiled cake. Bioresour Technol 165:336–342
63. Bhattacharjee N, Biswas AB (2021) Value-added fuels from the catalytic pyrolysis of Alternanthera philoxeroides. Fuel 295:120629
64. Jian X, Zhuang X, Li B, Xu X, Wei Z, Song Y, Jiang E (2018) Comparison of characterization and adsorption of biochars produced from hydrothermal carbonization and pyrolysis, Environ. Technol. Innovation 10:27–35
65. Han M, Jiang K, Jiao P, Ji Y, Zhou J, Zhuang W, Chen Y, Liu D, Zhu C, Chen X, Ying H, Wu J (2017) Bio-butanol sorption performance on novel porous-carbon adsorbents from corncob prepared via hydrothermal carbonization and post-pyrolysis method. Sci Rep 7:11753
66. Hale SE, Lehmann J, Rutherford D, Zimmerman AR, Bachmann RT, Shitumbanuma V, O'Toole A, Sundqvist KL, Arp HPH, Cornelissen G (2012) Quantifying the Total and Bioavailable Polycyclic Aromatic Hydrocarbons and Dioxins in Biochars. Environ Sci Technol 46:2830–2838
67. Zhang YZ, Xu MQ, Liang SX, Feng ZY, Zhao J (2021) Mechanism of persulfate activation by biochar for the catalytic degradation of antibiotics: Synergistic effects of environmentally

persistent free radicals and the defective structure of biochar. Sci Total Environ 794:148707
68. Zhang YZ, Xu MQ, Liu XK, Wang M, Zhao J, Li SY, Yin MC (2021) Regulation of biochar mediated catalytic degradation of quinolone antibiotics: Important role of environmentally persistent free radicals. Bioresour Technol 326:124780
69. Qin J, Qian S, Chen Q, Chen L, Yan L, Shen G (2019) Cow manure-derived biochar: Its catalytic properties and influential factors. J Hazard Mater 371:381–388
70. Fang G, Zhu C, Dionysiou DD, Gao J, Zhou D (2015) Mechanism of hydroxyl radical generation from biochar suspensions: Implications to diethyl phthalate degradation. Bioresour Technol 176:210–217
71. Zhang L, Cheng H, Pan D, Wu Y, Ji R, Li W, Jiang X, Han J (2021) One-pot pyrolysis of a typical invasive plant into nitrogen-doped biochars for efficient sorption of phthalate esters from aqueous solution. Chemosphere 280:130712
72. Mondal P, Majumder CB, Mohanty B (2006) Laboratory based approaches for arsenic remediation from contaminated water: Recent developments. J Hazard Mater 137:464–479
73. Duan X, Zhang C, Srinivasakannan C, Wang X (2017) Waste walnut shell valorization to iron loaded biochar and its application to arsenic removal. Resour-Effic Technol 3:29–36
74. Chen D, Wang X, Wang X, Feng K, Su J, Dong J (2020) The mechanism of cadmium sorption by sulphur-modified wheat straw biochar and its application cadmium-contaminated soil. Sci Total Environ 714:136550
75. Lee Y-E, Jo J-H, Kim I-T, Yoo Y-S (2018) Influence of NaCl Concentration on Food-Waste Biochar Structure and Templating Effects. Energies 11:2341
76. Yang K, Yang J, Jiang Y, Wu W, Lin D (2016) Correlations and adsorption mechanisms of aromatic compounds on a high heat temperature treated bamboo biochar. Environ Pollut 210:57–64
77. Jin J, Sun K, Wu F, Gao B, Wang Z, Kang M, Bai Y, Zhao Y, Liu X, Xing B (2014) Single-solute and bi-solute sorption of phenanthrene and dibutyl phthalate by plant- and manure-derived biochars. Sci Total Environ 473–474:308–316
78. Anyika C, Abdul Majid Z, Ibrahim Z, Zakaria MP, Yahya A (2015) The impact of biochars on sorption and biodegradation of polycyclic aromatic hydrocarbons in soils—a review. Environ Sci Pollut Res 22:3314–3341
79. Schmidt MWI, Noack AG (2000) Black carbon in soils and sediments: Analysis, distribution, implications, and current challenges. Glob Biogeochem Cycle 14:777–793
80. Eduah JO, Henriksen SW, Nartey EK, Abekoe MK, Andersen MN (2020) Nonlinear sorption of phosphorus onto plant biomass-derived biochars at different pyrolysis temperatures. Environ Technol Innovation 19:100808
81. Chen X, Chen G, Chen L, Chen Y, Lehmann J, McBride MB, Hay AG (2011) Adsorption of copper and zinc by biochars produced from pyrolysis of hardwood and corn straw in aqueous solution. Bioresour Technol 102:8877–8884
82. Zeng Z-W, Tan X-F, Liu Y-G, Tian S-R, Zeng G-M, Jiang L-H, Liu S-B, Li J, Liu N, Yin Z-H (2018) Comprehensive Adsorption Studies of Doxycycline and Ciprofloxacin Antibiotics by Biochars Prepared at Different Temperatures. Front Chem 6:80
83. Zhu X, Wang Y, Zhang Y, Chen B (2018) Reduced bioavailability and plant uptake of polycyclic aromatic hydrocarbons from soil slurry amended with biochars pyrolyzed under various temperatures. Environ Sci Pollut Res 25:16991–17001
84. Ma X, Anand D, Zhang X, Talapatra S (2011) Adsorption and Desorption of Chlorinated Compounds from Pristine and Thermally Treated Multiwalled Carbon Nanotubes. J Phys Chem C 115:4552–4557
85. Borisover MD, Graber ER (1997) Specific interactions of organic compounds with soil organic carbon. Chemosphere 34:1761–1776
86. Popovych N, Kyriienko P, Soloviev S, Baran R, Millot Y, Dzwigaj S (2016) Identification of the silver state in the framework of Ag-containing zeolite by XRD, FTIR, photoluminescence, 109Ag NMR, EPR, DR UV-vis, TEM and XPS investigations. Phys Chem Chem Phys 18:29458–29465
87. Jing F, Sohi SP, Liu Y, Chen J (2018) Insight into mechanism of aged biochar for adsorption of PAEs: Reciprocal effects of ageing and coexisting Cd2+. Environ Pollut 242:1098–1107
88. Ouyang D, Yan J, Qian L, Chen Y, Han L, Su A, Zhang W, Ni H, Chen M (2017) Degradation of 1,4-dioxane by biochar supported nano magnetite particles activating persulfate. Chemosphere 184:609–617
89. Wang X, Feng J, Cai Y, Fang M, Kong M, Alsaedi A, Hayat T, Tan X (2020) Porous biochar modified with polyethyleneimine (PEI) for effective enrichment of U(VI) in aqueous solution. Sci Total Environ 708:134575
90. Abdoul Magid ASI, Islam MS, Chen Y, Weng L, Li J, Ma J, Li Y (2021) Enhanced adsorption of polystyrene nanoplastics (PSNPs) onto oxidized corncob biochar with high pyrolysis temperature. Sci Total Environ 784:147115

Publisher's note Springer Nature remains neutral with regard to jurisdictional claims in published maps and institutional affiliations.